Journal of
Marine Science and Engineering

MDPI

Article

Performance of an Array of Oscillating Water Column Devices in Front of a Fixed Vertical Breakwater

Dimitrios N. Konispoliatis

Laboratory for Floating Structures and Mooring Systems, Division of Marine Structures, School of Naval Architecture and Marine Engineering, National Technical University of Athens, 9 Heroon Polytechniou Avenue, GR 157 73 Athens, Greece; dkonisp@naval.ntua.gr

Received: 22 October 2020; Accepted: 10 November 2020; Published: 12 November 2020

Abstract: The present study explores the performance of an array of cylindrical oscillating water column (OWC) devices, having a vertical symmetry axis, placed in front of a bottom seated, surface piercing, vertical breakwater. The main goal of this study is the investigation of a possible increase in the power efficiency of an OWC array by applying, in the vicinity of the array, a barrier to the wave propagation, aiming at amplifying the scattered and reflected waves originating from the presence of the devices and the wall. To cope with the set goal, a theoretical analysis is presented in the framework of linear potential theory, based on the solution of the proper diffraction, and pressure-radiation problems in the frequency domain, using the image theory, the matched axisymmetric eigenfunction expansion formulation, and the multiple scattering approach. Numerical results are presented and discussed in terms of the expected power absorption by the OWCs comparing different array's characteristics i.e.,: (a) angle of incidence of the incoming wave train; (b) distances from the breakwater; and (c) geometric characteristics of the different arrangements. The results show that compared to the isolated OWC array (i.e., no presence of the wall), the power efficiency of the OWCs in front of a breakwater is amplified at specific frequency ranges.

Keywords: breakwater; oscillating water column device; OWC array; absorbed wave power; power performance

1. Introduction

Sea waves have enormous power, therefore the construction of structures for mitigating such power is not easily accomplished. Breakwaters are widely used in coastal and offshore engineering, frequently applied in coastal protection and restoration schemes. They are barriers, either water-surface piercing or submerged, that are frequently displaced perpendicularly to the dominant direction of the incoming waves, which absorb, diffract, and reflect part of the wave energy, reducing the amount of energy that reaches the shoreline.

Breakwaters are primarily classified according to their structural features as restrained to the wave impact (fixed) or floating structures, whereas under these broad classifications, they can be further subdivided regarding their construction materials, shape, etc. [1]. Specifically, concerning the fixed breakwaters, they operate by reflecting the incoming wave train, as a bottom mounted rigid structure. Rubble mound, seawall, and barrier types of breakwaters fall in this category. Rubble mound breakwaters have probably existed for around 3000 years [2] and they are still applied for sheltering coastlines from wave action. Construction of breakwaters during the ancient time around the Mediterranean Sea was done by blocky stones, sometimes cementitious infill [3], while in recent times, numerous design methods for hydraulic performance and structural stability of rubble mound breakwaters have been developed i.e., [4–7]. A seawall breakwater is a most common defensive structure, acting as one large solid block at locations where the ocean environments are dominating

at the coast. It is usually composed of prefabricated reinforced concrete caissons, representing a better alternative in terms of performance, construction rapidity, standardization, environmental implications, and construction and maintenance costs when compared with the rubble mound type [8]. Many analytical and laboratory studies and field observations have been undertaken concerning the design and construction of vertical breakwaters (seawalls). Indicative, recent studies are [9–11]. On the other hand, in situations where the complete protection from the waves is not required, thin barriers, impermeable or permeable, supported with piles can be used as breakwaters. Pile breakwaters comprise a series of piles which partially attenuate the wave energy due to turbulences and eddies created around the solids, preventing also effectively the soar from sediment siltation [12–14]. In addition, barrier type of breakwater consists of perforated and slotted structures, operating as permeable breakwaters, increasing wave reflection as their porosity increases [15,16].

Although a breakwater structure is constructed to minimize the wave action in areas behind of it, in front of the structure the incoming wave energy is amplified due to the scattered and reflected waves originating from the presence of the vertical wall. This phenomenon has triggered increased interest on wave energy conversion systems operating near and/or on a breakwater. Moreover, the installation of wave energy converters (WEC) in front and/or on breakwaters is facilitated by easier electricity transmission to the mainland, allowing for common usage of infrastructure (i.e., electrical cable, power transfer equipment, etc.).

In the context of a breakwater-WEC system, numerous projects and studies have been presented globally, emphasizing the wall's positive effect on the converter's efficiency. Although several different types of WECs are under development, only few typologies have been commonly used in conjunction with coastal protection structures, namely (a) the overtopping devices (OTD); (b) the oscillating wave surge converter (OWSG); (c) the point absorbers (i.e., heaving devices); and (d) the oscillating water column devices (OWC).

Rubble mound breakwater-OTDs utilize a frontal sloping plate that leads the incident waves to overtop into one or more storage basins placed at a higher level than the seawater level. In its natural way back to the sea, the water passes through turbines, generating electricity [17]. Indicative studies concerning the design optimization of an OTD for efficiency maximization are [18–21]. Regarding the OWSC operation, the converter typically has one end fixed to the sea bed while the other end is free to move. The wave energy is absorbed by the relative motion of the body (i.e., the converter comes in the form of floats, flaps, or membranes) compared to the fixed point. Analytical formulations on the effect of an onshore barrier (i.e., a straight coast and a vertical breakwater) on the device's efficiency are presented in [22,23].

As far as point absorber devices are concerned, they gain the energy from their oscillation in heave direction, which is driven by means of their interaction with the wave field. The arrangement of a breakwater-heaving device system involves partial-floating bodies placed parallel to the predominant wave direction, in front of a vertical seawall. The bodies' movements due to the scattered and radiated waves from the array's members and their interaction with the vertical wall, allows the conversion of the floaters' kinetic energy to electricity using hydraulic or mechanical transmission [24]. Most recent indicative studies concerning hydrodynamic analysis and efficiency estimation of arrays of heaving devices placed in front of a linear vertical wall are presented in [25,26].

An OWC device is a partially submerged, hollow structure open to the seabed below the water line. The vertical motion of the sea surface alternatively pressurizes and depressurizes the air inside the OWC's chambers, generating a reciprocating flow through a self-rectifying turbine which is installed beneath the roof of the device. Looking towards the multi abilities provided by the breakwater-OWC system, several different designs have been presented in the literature, while most of them concern OWCs integrated at a vertical breakwater. Specifically, in [27,28], a theoretical study of an OWC standing at the tip of a breakwater and along a straight coast is presented, respectively, whereas in [29–31], an OWC integrated at a flat breakwater is theoretically and experimentally investigated. In [32,33], a detailed analysis concerning the structural and economic feasibility of integrated OWC within a

Mediterranean port is presented and in [34], a linearized theory of an array OWC installed on a straight coast is described. In addition, the effect of a breakwater on OWC performance using CFD analysis under the action of regular and irregular waves is presented in [35]. Finally, in [36], a modified integrated breakwater-OWC system is investigated using numerical and experimental simulations in terms of its power performance. As far as the performance of an OWC device placed in front of a vertical breakwater is concerned, only few studies are presented in the literature. In [37], a theoretical analysis of a vertical OWC device placed in front of a vertical wall is presented, whereas in [38], the efficiency of an array of five OWCs placed in parallel direction to a vertical breakwater is examined, for installation at the port of Heraklion (i.e., Crete island).

The scope of this work is to examine the effect of a bottom mounted, surface piercing, breakwater of infinite length, on the power efficiency of an array of OWCs placed in a random location in front of the wall. The examined converters consist of an exterior partially immersed toroidal body supplemented by a coaxial interior, bottom mounted, free-surface piercing vertical cylinder. In the annulus between the internal cylinder and the external torus, a finite volume air chamber is formed in which the oscillating air pressure is developed. An analogous OWC type has been examined to operate alone in the open sea, combined with a wind turbine supported on the converter's interior concentric cylindrical body, and as part of a Jacket platform [39–42]. A theoretical model is presented, taking into account the wave hydrodynamic interactions among the OWCs and the fluid flow in front of the breakwater. Several distances between the bodies and the breakwater are examined, along with different array configurations (i.e., OWCs in a rectangular, parallel, and perpendicular arrangement to the front wall) and wave heading angles, to assess the array's efficiency towards its optimization. The presented results show that the power efficiency of an array of OWCs in front of a breakwater is amplified compared to the one in unbounded waters (i.e., without the presence of the vertical wall).

This work is organized as follows: Section 2 describes the solution of the corresponding diffraction and pressure-radiation problems, while in Section 3, the OWCs' hydrodynamic characteristics and absorbed power are presented. Section 4 provides and discusses the numerical results and finally the conclusions are drawn in Section 5.

2. Formulation of the Hydrodynamic Problem

The diffraction and the pressure-radiation problems under consideration are examined within the context of the arrangement shown in Figure 1. An array of N similar OWCs is assumed, situated in the vicinity of a vertical, bottom-mounted, surface piercing, breakwater of infinite length. The water depth is denoted by h, assuming the sea bottom flat and horizontal. The outer and inner radii of each device's chamber are denoted by α, b, respectively, whereas the distance between the bottom of the external torus and the seabed is denoted by h_c. The radius of the interior, bottom seated, coaxial cylindrical body is denoted by c. In addition, the distance between the center of the closest to the wall converter and the breakwater is denoted by L_w, whereas the distance between adjacent OWCs is by L_b. Small amplitude harmonic waves (with angular frequency ω, wave height H, and wave length λ) are incident to the breakwater at an angle β. A global, right-handed Cartesian co-ordinate system O-xyz is introduced with origin located at the bottom of the breakwater, with its vertical axis Oz directed upwards, while N local cylindrical co-ordinate systems $\left(r_q, \theta_q, z\right)$, $q = 1, 2, \ldots, N$ are defined with origins at the intersection $\left(X_q, Y_q\right)$ of the sea bottom with the vertical axis of symmetry of each converter. The geometric layout of the breakwater-OWC system is illustrated in Figure 1.

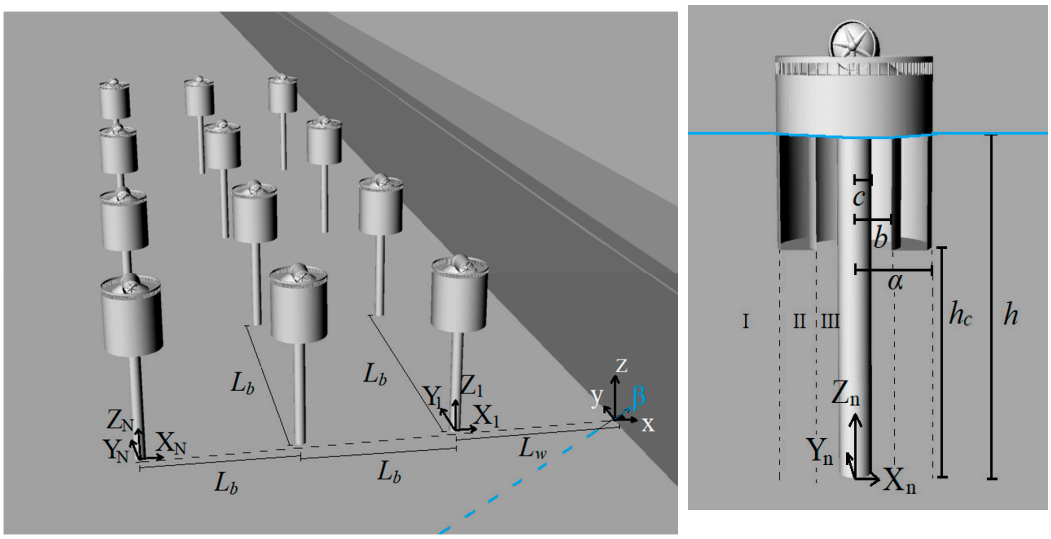

(**a**) (**b**)

Figure 1. 3D representations of an OWC array in front of a breakwater: (**a**) array of *N*-OWCs in front of a breakwater; (**b**) schematic representation of the examined OWC, side view-xz.

In the present analysis, the fluid is assumed non viscous and incompressible and the water flow irrotational so that linear water wave theory may be employed. Under this assumption, the fluid flow around each device q, q = 1, 2, … , N, described by the potential function: $\Phi\left(r_q, \theta_q, z_q; t\right) = Re\left[\varphi\left(r_q, \theta_q, z_q\right)e^{-i\omega t}\right]$ can be decomposed on the basis of linear modeling as [43]:

$$\varphi\left(r_q, \theta_q, z_q\right) = \underbrace{\varphi_0\left(r_q, \theta_q, z_q\right) + \varphi_s^q\left(r_q, \theta_q, z_q\right)}_{\varphi_D^q} + \sum_{p=1}^{N} p_{in0}^p \varphi_p^{qp}\left(r_q, \theta_q, z_q\right) \quad (1)$$

In Equation (1), φ_0 stands for the velocity potential of the undisturbed incident harmonic wave; φ_s^q is the scattered potential around the q OWC, assuming atmospheric air pressure inside the chamber; φ_p^{qp} denotes the pressure-dependent radiation potential around the q OWC when it is considered as an open-duct body (i.e., atmospheric air pressure inside the chamber) due to unit air pressure, p_{in0}^p, in the chamber of the p device. The term $\varphi_D^q = \varphi_0 + \varphi_s^q$ denotes the diffracted component of the corresponding total wave potential around the q body.

The potentials $\varphi\left(r_q, \theta_q, z_q\right)$ are solutions of the Laplace equation in the entire fluid domain and satisfy the proper boundary conditions on the sea bed and the water free surface; the kinematic conditions on the mean body's wetted surface and the no-flux boundary condition on the breakwater's surface [44]:

$$\frac{\partial \varphi}{\partial X_q} = 0 \text{ at } X_q = 0 \quad (2)$$

In the present study, the method of images is applied together with the assumption of a fully reflecting breakwater. Specifically, the presence of the breakwater in front of the OWC array is represented by taking into consideration the image "virtual" devices with respect to the wall, without the presence of the wall. The equivalent array of 2N devices is exposed to the action of two-directional surface waves (i.e., one propagating at angle β and a second at angle 180-β) [23,37] (see Figure 2). Herein, based on the method of images, 2N local cylindrical co-ordinate systems

(r_q, θ_q, z), $q = 1, 2, \ldots, 2N$ are defined with origins at the intersection (X_q, Y_q) of the sea bottom with the vertical axis of symmetry of each OWC. Thus, Equation (1) can be written as:

$$\varphi(r_q, \theta_q, z_q) = \underbrace{\varphi_0(r_q, \theta_q, z_q) + \varphi_s^q(r_q, \theta_q, z_q)}_{\varphi_D^q} + \sum_{p=1}^{2N} p_{in0}^p \varphi_p^{qp}(r_q, \theta_q, z_q) \quad (3)$$

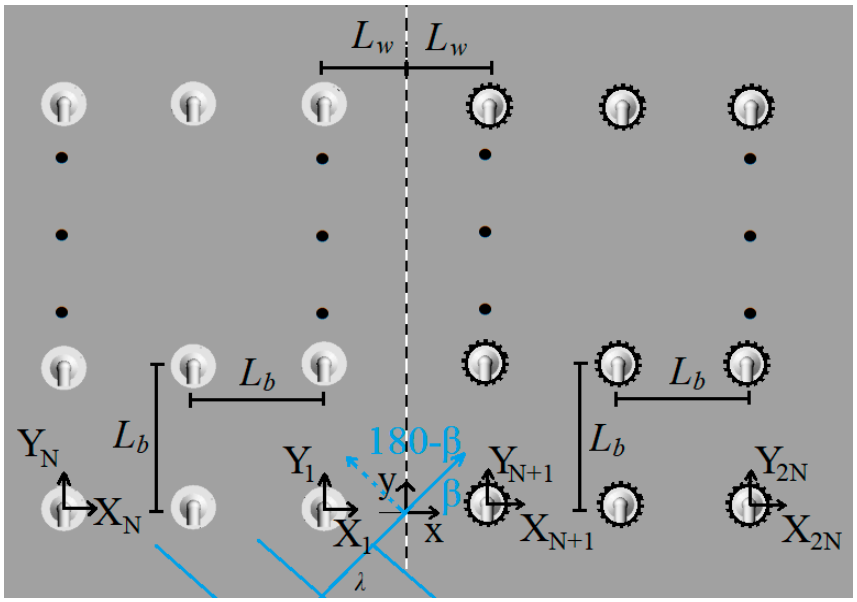

Figure 2. 2D plane representation of a breakwater-OWC system using the method of images. The image devices are denoted dashed.

In Equation (3), φ_0, φ_s^q, φ_p^{qp} correspond to the velocity potential of the undisturbed incident harmonic wave; the scattered potential around the q, OWC, $q = 1, 2, \ldots, 2N$, and the pressure-dependent radiation potential around the q OWC $q = 1, 2, \ldots, 2N$, respectively. In addition, p_{in0}^p, corresponds to the air pressure in the chamber of the p device, $p = 1, 2, \ldots, 2N$.

The velocity potentials of Equation (3) are solutions of the Laplace equation and they have to satisfy the below boundary conditions:

(a) on the water free surface:

$$\begin{cases} \omega^2 \varphi_j^q - g \frac{\partial \varphi_j^q}{\partial z} = 0, \ j = 0, s; \ z = h; \ r_q \geq a; \ c \leq r_q \leq b \\ \omega^2 \varphi_P^{qp} - g \frac{\partial \varphi_P^{qp}}{\partial z} = \begin{cases} 0, \ r_q \geq a \\ -\delta_{q,p} \frac{i\omega}{\rho}, \ c \leq r_q \leq b \end{cases} ; \end{cases} \quad (4)$$

(b) on the sea bottom:

$$\frac{\partial \varphi_k^i}{\partial z} = 0, \ i = p, qp; \ k = 0, s, P; \ z = 0; \quad (5)$$

(c) kinematic condition on the mean device's wetted surface:

$$\begin{cases} \frac{\partial \varphi_s^q}{\partial n^q} = -\frac{\partial \varphi_0^q}{\partial n^q} \\ \frac{\partial \varphi_p^{qp}}{\partial n^q} = 0 \end{cases} \quad (6)$$

Finally, a radiation condition stating that propagating disturbances must be outgoing is imposed.

In Equation (4), g is the gravitational acceleration; ρ is the water density; $\delta_{q,p}$ is the Kronecker's symbol. In addition, in Equation (6), the $\frac{\partial()}{\partial n^q}$ term denotes the derivative in the direction of the outward unit normal vector n^q, to the mean wetted surface S_0^q on the q OWC.

The wave interaction phenomena among the OWCs (i.e., initial and image solids) have been taken into consideration through the physical idea of multiple scattering. Specifically, by properly superposing the incident wave potential and the propagating and evanescent modes that are scattered and radiated by the OWC's, exact representations of the fluid's velocity potentials around each device can be obtained, based on the single device hydrodynamic characteristics. The latter are derived through the use of matched axisymmetric eigenfunction expansions [45] for the velocity potential around each single OWC, considered alone in the wave field. Based on this method, the flow field around each OWC is subdivided in coaxial ring-shaped fluid regions, defined as *I*, *II*, *III*, (see Figure 1b) in each of which appropriate series representations of velocity potential can be established. These series representations are solutions of Laplace equation; satisfy the Equations (4)–(6); the radiation condition at infinity and the continuity relation, of the velocity potentials and their radial derivatives, at the vertical boundaries of neighborhood fluid regions.

The method for the solution of the diffraction and the pressure-radiation problems of a single OWC device along with the implementation of the multiple scattering approach on array of OWCs has been thoroughly described in [46]. Nevertheless, by the way of example, the velocity potentials around an isolated OWC device are presented in the Appendix A.

3. Array's Efficiency

Due to the water oscillation inside the OWCs' chambers, the dry air above the free surface is pushed through an air turbine, located at the top of the chamber, producing an air volume flow inside each chamber, denoted as $Q\left(r_q, \theta_q, z_q; t\right) = Re\left\{\mathrm{q}\left(r_q, \theta_q, z_q\right) e^{-i\omega t}\right\}$. Here, q equals to:

$$\mathrm{q} = \iint\limits_{S_i} u_z^q dS_i = \iint\limits_{S_i} \frac{\partial \varphi}{\partial z} dS_i \tag{7}$$

The term u_z^q denotes the vertical velocity of the water surface in the q OWC, $q = 1, 2, \ldots, N$; S_i is the cross-sectional area of the inner water surface inside the q device; and φ is the velocity potential inside the OWCs' chambers (i.e., *III* fluid domain).

Since the velocity potential around each device of the array can be described as a superposition of the diffraction and the pressure-radiation velocity potentials (see Equation (1)), similarly the air volume flow q inside the q OWC, $q = 1, 2, \ldots, N$, can be written in the form:

$$\mathrm{q}\left(r_q, \theta_q, z_q\right) = \mathrm{q}_D^q\left(r_q, \theta_q, z_q\right) + \sum_{p=1}^{N} p_{in0}^p \mathrm{q}_p^{qp}\left(r_q, \theta_q, z_q\right) \tag{8}$$

In Equation (8), the term q_D^q stands for the diffraction air volume flow, while q_p^{qp} denotes the pressure-dependent volume flow, known as radiation admittance [47].

The radiation admittance of the q OWC $q = 1, 2, \ldots, N$ due to unit air pressure head inside the p device, $p = 1, 2, \ldots, N$ can be also written as a function of the radiation conductance and the radiation susceptance coefficients, i.e.,:

$$\mathrm{q}_p^{qp} = -g_p^{qp} + i f_p^{qp} \tag{9}$$

Based on the method of images, the considered breakwater-OWC system interacting with an incident wave of angle β, is equivalent to an array of $2N$ devices, mirror between each other with respect to the breakwater, which are exposed to the action of two wave trains at angles β and $180-\beta$, without the presence of the vertical wall. Thus, the diffraction volume flow inside the q OWC $q = 1, 2, \ldots, N$,

equals to the sum of the corresponding diffraction volume flows inside the q device for wave angle propagation β and 180-β, denoted as $q_D^{q,\beta}$ and $q_D^{q,180-\beta}$, respectively, when the device is assumed part of an array of $2N$ bodies, i.e.,:

$$q_D^q = q_D^{q,\beta} + q_D^{q,180-\beta} \tag{10}$$

Here, the terms $q_D^{q,k}$, $k = \beta,\ 180-\beta$ are derived from Equation (7) for every examined wave heading angle.

The radiation admittance, q_p^{qp}, of the q OWC device, q = 1, 2, ..., N, placed in front of a vertical wall can be also derived through the method of images. More specific, the radiation conductance and the radiation susceptance coefficients of the q OWC, q = 1, 2, . . . , N due to unit air pressure head inside the p OWC, p = 1, 2, . . . , N can be derived by summing properly the radiation conductance and susceptance coefficients of the q OWC q = 1, 2,..., N, due to unit air pressure head inside the p OWC, p = 1, 2, . . . , N with the corresponding coefficients of the q OWC q = 1, 2,..., N, due to unit air pressure head inside the p OWC's image device, denoted as p', $p' = N + 1, \ldots, 2N$ [37,38].

In the present paper, an air turbine is assumed to be placed in the OWCs' ducts, between the chamber and the outer atmosphere that exhibits an approximately linear relationship between the inner air pressure and the volume flow (e.g., a Wells type air turbine) i.e.,:

$$q = \Lambda\, p_{in0}^q \tag{11}$$

Here, Λ represents the complex pneumatic admittance of the air turbine [48]. The real part of Λ is related to the pressure drop through the turbine, whereas the imaginary part represents the effect of air compressibility inside the chamber. In the presented numerical results (see Section 4), the pneumatic admittance of the air turbine is assumed to attain an optimum value, Λ_{opt}, as presented in [49], which maximizes the power efficiency of a similar OWC device, considered alone in the wave field, without the presence of the breakwater.

Having determined all the pressure coefficients of an array of N OWCs in front of a vertical breakwater, each devices' wave absorbed power, $P^q,\ q = 1, 2, \ldots, N$ can be written as:

$$P^q(\omega) = \frac{1}{2}\Lambda_{opt}\left| p_{in0}^q \right|^2 \tag{12}$$

Here, ω stands for the wave frequency.

In Equation (12), the P^q term denotes the efficiency of the q OWC device since in the present paper, the losses that occur in the energy conversion chain are not taken into consideration.

To evaluate the constructive or destructive effect of a vertical seawall on the WECs' power efficiency, a "q-factor", q_f, is introduced which is defined as the ratio of the total wave power absorbed by the OWC array to N (the number of OWCs in the array) times the absorbed power by the same converter in isolation condition [26,50]. Thus, it holds:

$$q_f = \frac{\text{total absorbed power by the array of } N \text{ OWC placed in front of a vertical breakwater}}{N \times \text{ absorbed power by the OWC in isolation condition without a breakwater}} \tag{13}$$

For $q_f > 1$, the scattered and reflected waves due to the presence of the solids and the vertical wall have a constructive effect on the array's efficiency, increasing the value of the total absorbed wave power compared to the corresponding efficiency of N OWCs placed in isolation (alone in the wave field). On the other hand, when $q_f < 1$, the wave interaction phenomena between the devices and the breakwater have a destructive effect on the amount of the array's efficiency compared to the wave absorbed power by N number of isolated OWCs.

4. Numerical Results

4.1. Test Cases

The theoretical method described in the present paper is applied to an array of OWCs placed in front of a breakwater. The examined converter's external and inner radii equal to α and $b = 0.9\alpha$, respectively. The distance between the bottom of the external torus and the seabed equals to h_c and the water depth equals to $h = 7.14\alpha$. Concerning the inner cylindrical body, it is assumed to be sea bottom seated with a radius of $c = 0.4\alpha$ The OWCs' air turbine characteristics are considered to be equal to the Λ_{opt} value of a similar OWC in isolation condition at its pumping resonance wave frequency [51], whereas the distance between the center of the closest to the wall converter and the breakwater is L_w, and the distance between adjacent OWCs is $L_b = 4\alpha$ (see Figures 1 and 2).

The calculation of the Fourier coefficients of the velocity potentials (see Appendix A) around each OWC device in the array is the most significant part of the presented theoretical analysis because of their influence on the accuracy solution. Here, for the *I* and *III* ring elements $n = i = 60$, whereas for the *II* fluid domain $n = 100$. The considered number of modes are $m = \pm 7$ and the number of wave interactions were taken equal to 7. The presented numerical results were obtained using the in-house developed computer software HAMVAB [52]. The software being relied on analytical representations of the velocity potential around each cylinder-type OWC device of the array was preferred in the present contribution against other available numerical tools applicable to general 3D geometries, since by keeping the same accuracy with them, it is usually less CPU time-consuming (i.e., for the solution of the diffraction and radiation problem in each wave frequency a time of 40 s is required).

In the following subsections, the absorbed power by the OWC array is presented for several examined parameters, namely: (a) number of converters; (b) array orientation to the breakwater; (c) wave heading angles; (d) distances between the device and the breakwater; (e) device's draught; and (f) distances between the devices.

4.2. Effect of the OWCs Orientation to the Breakwater

In this subsection, the effect of the OWC-array orientation with respect to the breakwater on the array's efficiency is presented. The examined converters are placed in front of a vertical breakwater in: (a) parallel to the wall arrangement; (b) perpendicular to the wall arrangement; and (c) in a rectangular arrangement in front of the wall. Furthermore, in each of these arrangements, several numbers of OWC devices are considered, i.e., configurations 1, 2, 3, 4, 5. In Figure 3, the examined orientation of the OWC's arrays arrangements and the breakwater are depicted. Herein, the distance between the center of the closest to the wall converter and the breakwater equals to $L_w = 3\alpha$, whereas the distance between the bottom of the external torus and the seabed equals to $h_c = 6.14\alpha$.

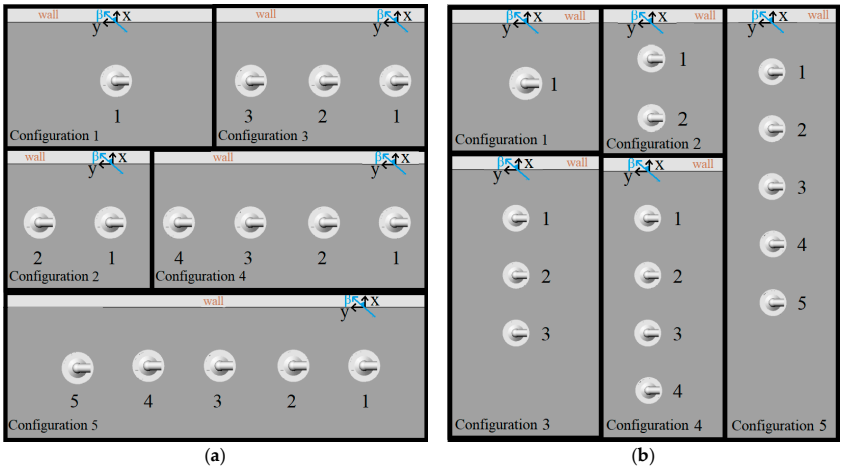

(a) (b)

Figure 3. *Cont.*

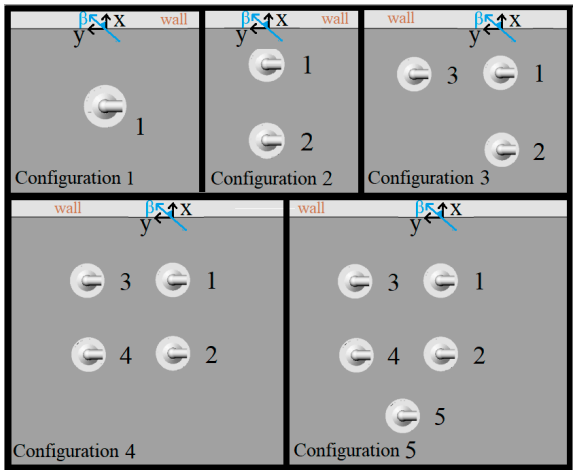

(**c**)

Figure 3. Schematic representations of the considered OWC array arrangements in front of a vertical breakwater and the numbering of the devices' considered: (**a**) five examined configurations of OWCs arranged in parallel direction to the wall; (**b**) five examined configurations of OWCs arranged perpendicularly to the wall; (**c**) five examined configurations of OWCs arranged rectangularly to the wall.

According to the presented analysis, the pumping resonance of the water column inside the oscillating chamber occurs at wave frequency equal to 2.62 [rad/s], for α = 1 m, thus the air turbine coefficient inside the OWCs equals to 10.60 [m^5/(kN.s)].

Figure 4 depicts the modulus of the inner air pressure head inside the 1st OWC of the array, i.e., $p^q_{in0}/(H/2)$, q = 1, normalized by the wave amplitude along with the q_f factor (as described in Equation (13)) for each examined OWC configuration for the parallel to the wall array arrangement. The results are plotted against the non-dimensional wave numbers, kα, in the range of k$\alpha \in$ [0.05, 1.5] and for wave heading angles β = 0, π/6, π/4 (i.e., here k stands for the wave number). Similarly, in Figures 5 and 6, the corresponding inner air pressure of the 1st OWC device and the q_f factor for the perpendicular and rectangular to the wall array arrangements, respectively, are presented.

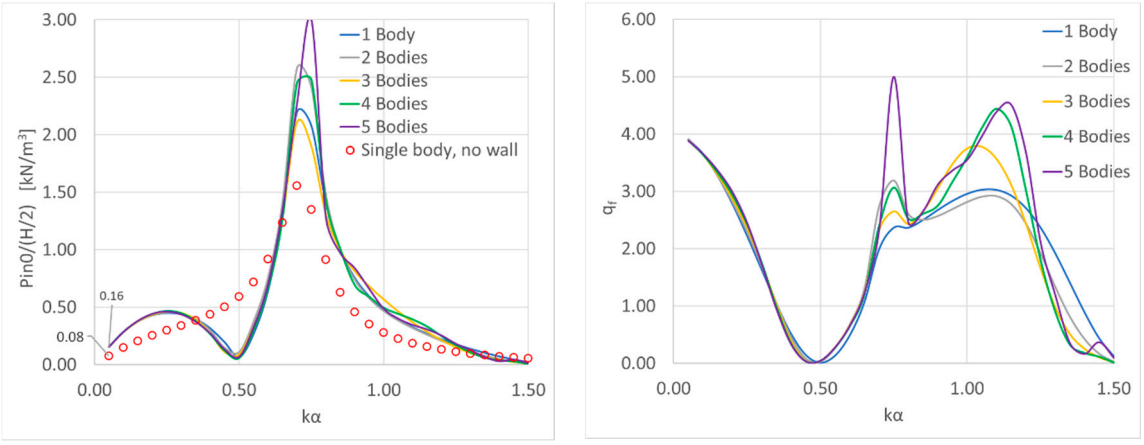

(**a**)

Figure 4. *Cont.*

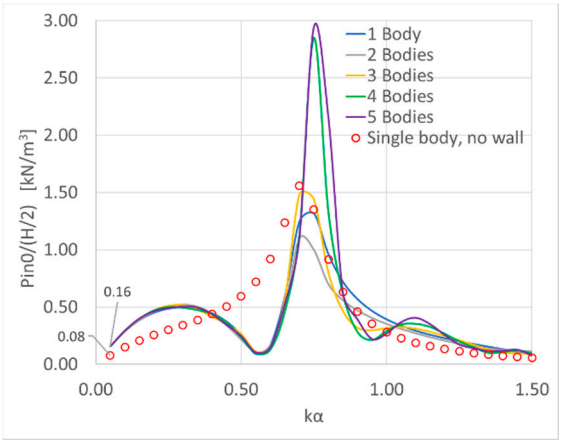

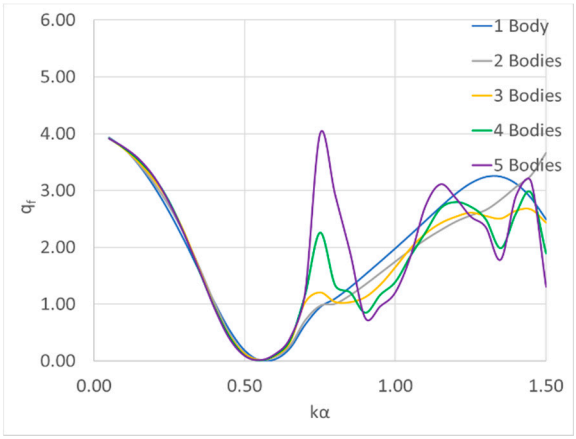

(**b**)

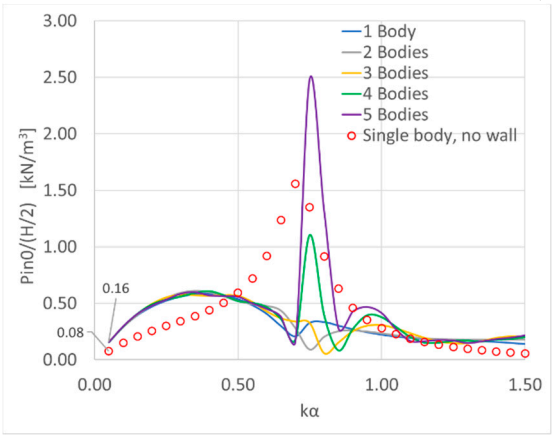

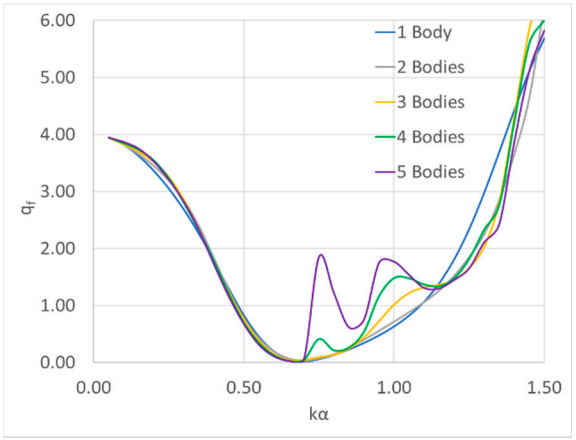

(**c**)

Figure 4. Air pressure inside the 1st OWC (left column figures) and array's q_f factor (right column figures) versus kα for various examined wave heading angles: (**a**) β = 0; (**b**) β = π/6; (**c**) β = π/4. Parallel arrangement.

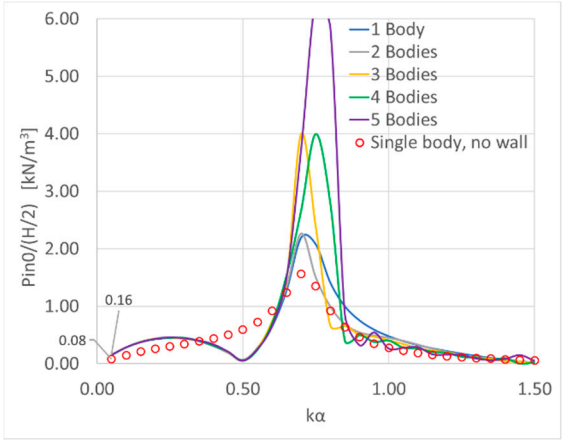

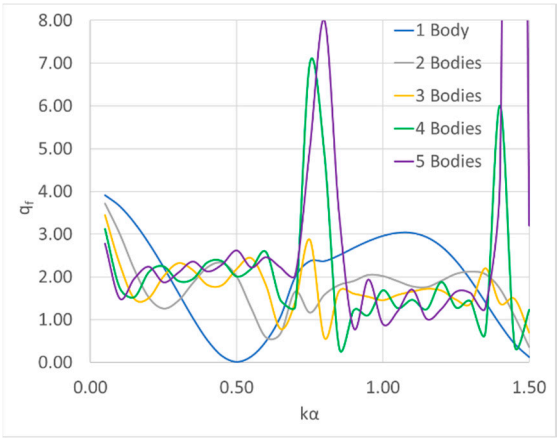

(**a**)

Figure 5. *Cont.*

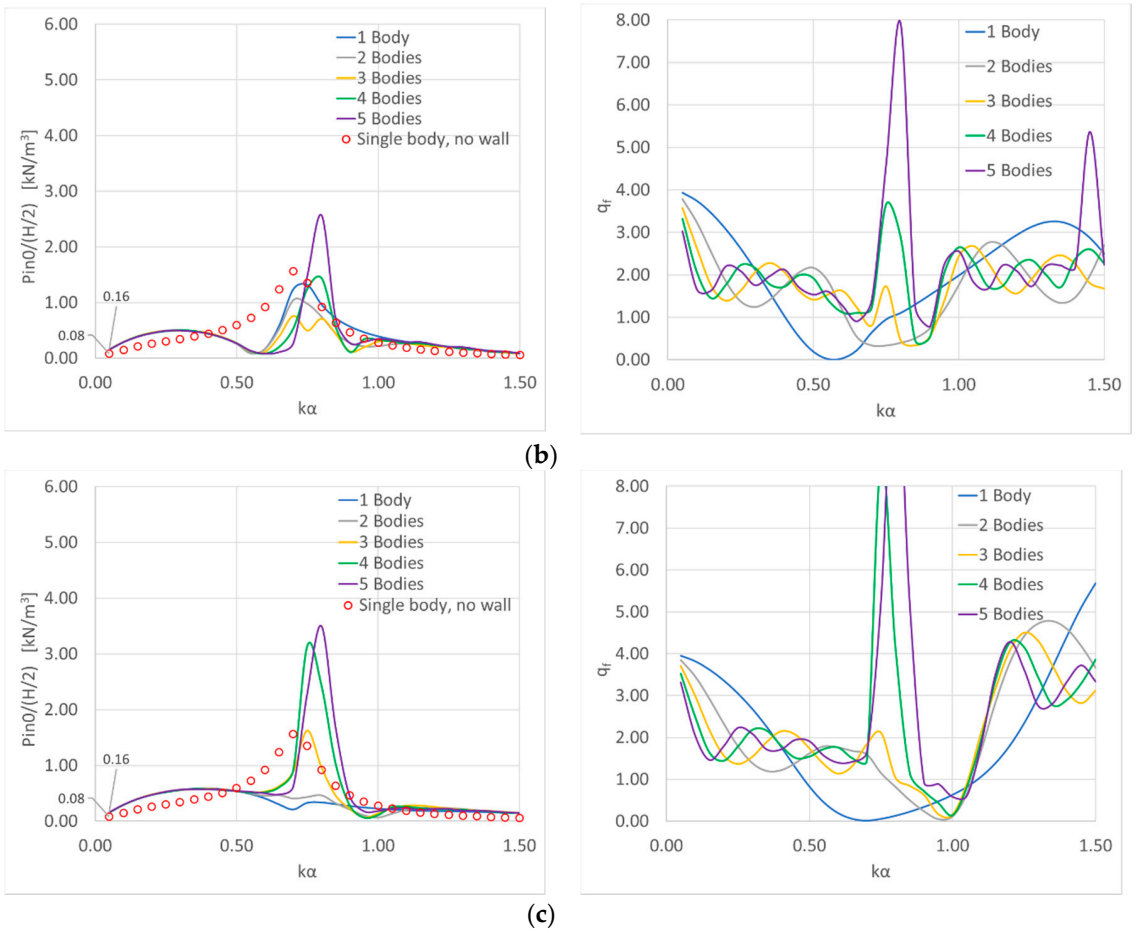

(**b**)

(**c**)

Figure 5. Air pressure inside the 1st OWC (left column figures) and array's q_f factor (right column figures) versus kα for various examined wave heading angles: (**a**) β = 0; (**b**) β = π/6; (**c**) β = π/4. Perpendicular arrangement.

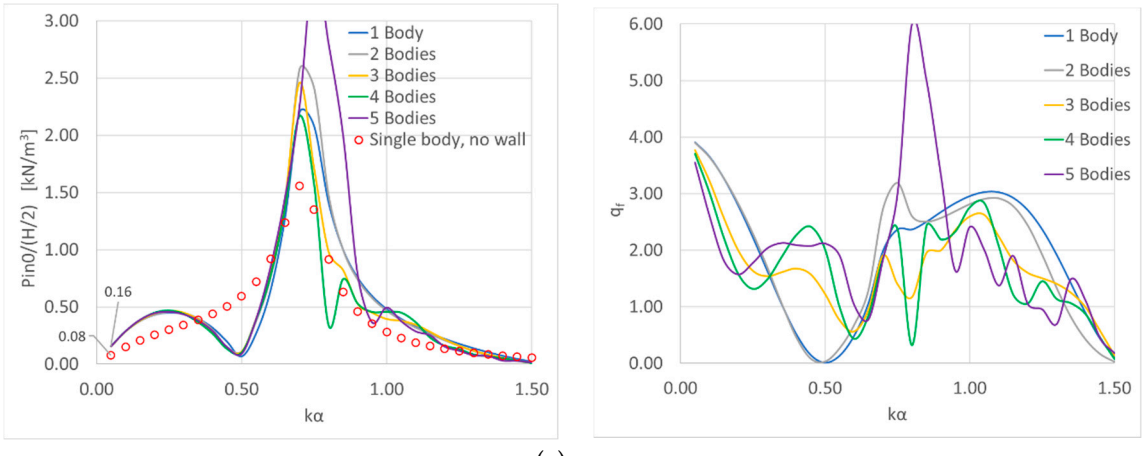

(**a**)

Figure 6. *Cont.*

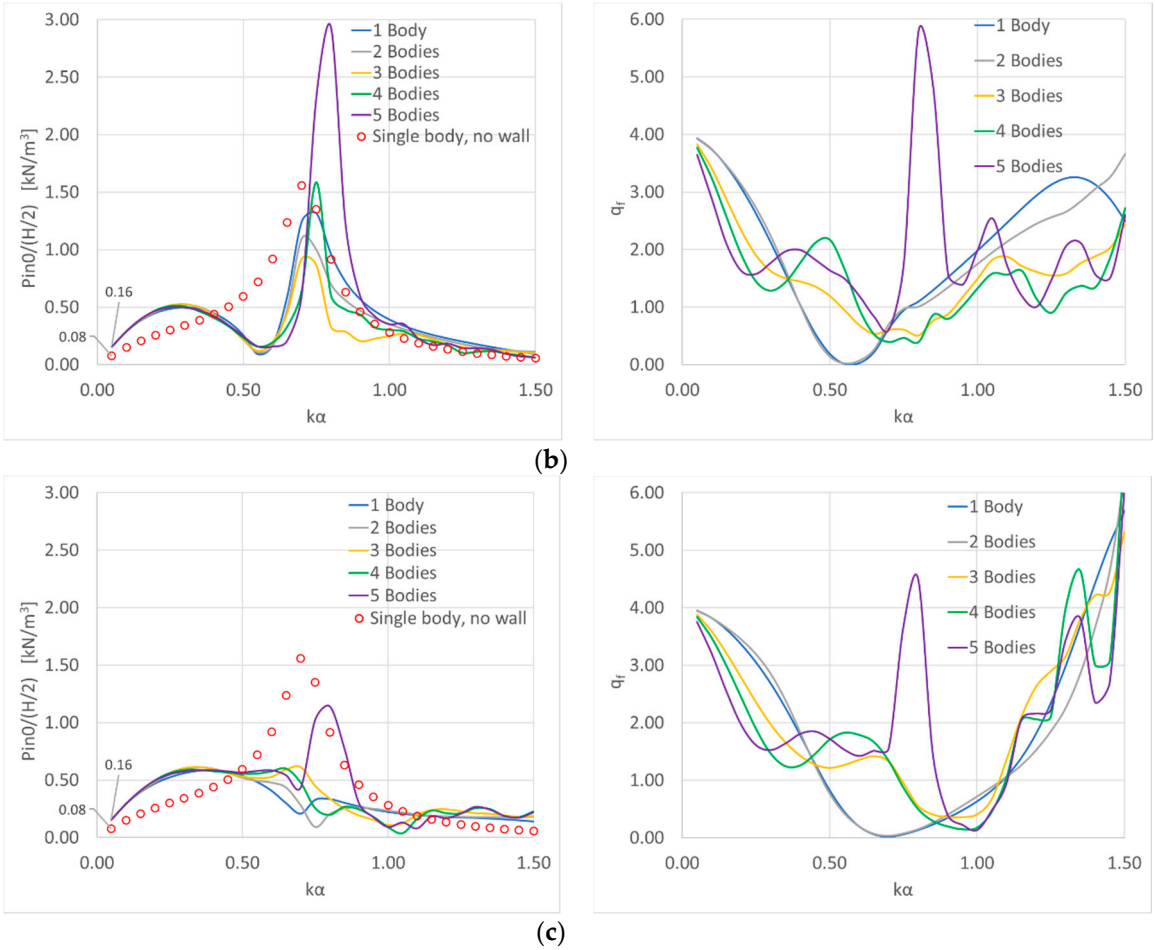

Figure 6. Air pressure inside the 1st OWC (left column figures) and array's q_f factor (right column figures) versus kα for various examined wave heading angles: (**a**) β = 0; (**b**) β = π/6; (**c**) β = π/4. Rectangular arrangement.

It can be seen from Figure 4 that the breakwater has a significant effect on the inner air pressure head of the 1st OWC device. The values of the air pressure inside the OWC in front of a breakwater do not follow a similar variation pattern to the corresponding values for the unbounded water case. Specifically, the values of the air pressure inside the OWC when placed in front of a breakwater attain almost two times larger values than those of the air pressure inside the same OWC, without, however, the presence of the breakwater, for kα tending to zero, at all the examined wave heading angles and OWC configurations (i.e., 1, 2, . . . , 5 number of bodies in front of the breakwater). Furthermore, it can be seen that the wave interaction phenomena between the OWCs and the vertical wall affect the values of the inner air pressure of the 1st converter also at higher values of kα. It is depicted that the inner air pressure tends to zero for kα values in the range of [0.5, 0.6] for β = 0; π/6; π/4. This behavior does not appear in the case of the isolated OWC without the presence of the wall. The zeroing of the air pressure head can be attributed to the standing wave due to the presence of the vertical breakwater and in particular it appears when the distance between the initial and the image converter equals to half wave length [53]. Furthermore, it is also notable that for kα ≈ 0.7, the inner air pressure of the converter, when it is considered part of an array or isolated in the wave field, exhibits a resonant peak regardless the wave heading angle. This resonance is associated with the pumping modes of the interior basin due to the existence of the moonpool [54]. As far as the number of the OWCs in each examined configuration is concerned, it can be seen that as the number of the OWCs in the array increases, the values of the inner air pressure inside the 1st OWC device attain an oscillatory behavior around the corresponding values of the single breakwater-OWC case, for large values of kα.

Concerning the effect of the breakwater on the array's power efficiency, it can be seen from the q_f factor figures, that this effect is constructive or destructive depends on the examined wave number. Specifically, at small wave numbers, the efficiency of the array is four times higher than the absorbed power by an isolated OWC (without the presence of the vertical wall). On the other hand, at $k\alpha \in [0.5, 0.6]$, the q_f factor attains values lower than one, thus the breakwater has a destructive effect on the array's power efficiency. Furthermore, at higher wave numbers, i.e., $k\alpha > 0.6$ the presence of the breakwater increases the array's absorbed power compared to the isolated case, since $q_f > 1$. Nevertheless, as the wave heading angle increases, the wave numbers in which $q_f > 1$ are sifted to higher values.

As far as the perpendicular arrangement of the OWCs in front of the breakwater is concerned, a similar conclusion to Figure 4 can be derived concerning the effect of the vertical wall on the values of the inner air pressure of the 1st OWC (i.e., the one closest to the breakwater). Specifically, as in the parallel arrangement case, for $k\alpha$ tending to zero, the doubling of the air pressure values for the breakwater-OWC case is also notable, compared to the no-wall case. In addition, the zeroing of the values at the wave number, which corresponds to a wavelength, equals to two times the distance between the initial and the image converter is presented here. Furthermore, the resonances at the pumping wave frequency, i.e., $k\alpha \approx 0.7$ are also depicted regardless of the number of the converters in the array. On the other hand, the q_f factor graphs do not follow the same pattern as the corresponding graphs in the parallel arrangement. It can be reported that the values of the q_f oscillate around the corresponding values of the single OWC-breakwater case. These oscillations become more pronounced as the number of the OWCs in the array increases and can be attributed explicitly to the scattered and reflected waves that seem to strongly affect the wave field around the converters with respect to the incident wave direction. Concerning the examined wave heading angles, it can be seen that the constructive effect of the breakwater on the array's efficiency, compared to the isolated OWC case, is increased as the values of the wave heading angle and the wave number increase. Furthermore, compared to the parallel OWC arrangement, here the q_f values do not zero at $k\alpha \in [0.5, 0.6]$, since the distances between the OWCs and the breakwater are not the same for each OWC (i.e., the distance between the initial and image converters does not correspond to half wave length for each OWC at this wave number band). As far as the remaining examined $k\alpha$ values are concerned, the q_f does not seem to attain significantly higher values than the corresponding factor of the parallel arrangement (see Figure 4), despite that the wave interactions between the bodies and the breakwater are amplified in this arrangement. Hence, it can be concluded that the increased interaction phenomena between the OWCs and the breakwater are not always beneficial for the array's efficiency at every wave frequency.

Continuing with the results of the rectangular arrangement, presented in Figure 6, it can be noted that the graphs of the air pressure inside the 1st OWC device follow a similar pattern as in the aforementioned arrangements (i.e., parallel and perpendicular). It is depicted that due to the presence of the breakwater, the air pressure attains double values than the no-wall case, at wave numbers tending to zero, regardless of the wave heading angle and the number of bodies in the array. Additionally, the resonance of the inner air pressure, at the pumping wave frequency i.e., $k\alpha \approx 0.7$, is notable. However, this resonance is dictated by the wave heading angle and the wave interaction phenomena between the converters and the vertical wall, since as the wave angle increases, the air pressure values at $k\alpha \approx 0.7$ decrease. Furthermore, the zeroing of the air pressure values at $k\alpha \in [0.5, 0.6]$ is also notable in the rectangular arrangement. This was also the case for the parallel and the perpendicular examined arrangements. Thus, it can be obtained that the wave number in which the OWC's inner air pressure zeros is affected by the device's distance from its image device and not by the examined array configuration and orientation to the wave impact. As far as the array's efficiency is concerned, it can be derived that for small wave numbers, the breakwater has a constructive effect on the array's power performance regardless of the examined body configuration, or array arrangement, attaining four times higher values of absorbed power than the no-wall cases. On the other hand, as the wave number increases, the distances between the devices and the vertical wall, as well as the wave

heading angles and the number of bodies in the array do not always have a constructive effect on the array's power efficiency.

In conclusion, when comparing the results from Figures 4–6, it can be obtained that for wave numbers tending to zero, the three examined configurations attain similar results. For wave numbers in the range of $k\alpha \in [0.1, 0.3]$, the parallel to the breakwater OWC arrangement performs better than the rectangular or perpendicular arrangements, attaining higher values of q_f. On the other hand, the breakwater has a destructive effect on the efficiency of the array arranged parallel to the vertical wall for wave numbers in the range of $k\alpha \in [0.5, 0.6]$, whereas for the rectangular and perpendicular array, the presence of the vertical wall has a positive impact on the array's power performance at the same wave number range. At wave numbers around the pumping resonance wave frequency, i.e., $k\alpha \approx 0.7$, the three examined arrangements attain similar q_f results. Nevertheless, the array's efficiency is increased as the number of bodies in the array increases. Finally, at large wave numbers i.e., $k\alpha > 1$, the array's power efficiency is mainly affected by the wave heading angle, i.e., the values of q_f increase as the wave heading angle increases.

4.3. Effect of the OWCs' Distance from the Breakwater

In this subsection, the effect of the distance between the OWCs' and the breakwater on their wave power efficiency is examined. Here, a parallel array arrangement of five similar OWCs in front of a breakwater is considered (see Configuration 5 in Figure 3a). The characteristics of the examined OWCs are presented in Section 4.1, whereas here, $h_c = 6.14\alpha$. The examined distances from the wall equal to $L_w = 3\alpha, 6\alpha, 9\alpha, 12\alpha$, and the wave heading angles to $\beta = 0, \pi/6, \pi/4$. Additionally, the air turbine coefficient inside the OWCs equals to 10.60 [m^5/(kN.s)].

Figure 7 depicts the modulus of the air pressure head inside the 1st OWC of the array, as well as the q_f factor for each examined distance between the devices and the breakwater and wave heading angles. It can be noted that the distance between the center of the devices and the breakwater significantly affects the air pressure head inside the 1st OWC device. Specifically, the values of the air pressure when the array is placed away from the wall (i.e., $L_w = 6\alpha, 9\alpha, 12\alpha$) oscillate around those of the $L_w = 3\alpha$ case. It can be also seen that the larger the distance of the converters from the wall is, the stronger the oscillatory behavior of the air pressure RAOs. As far as the examined wave heading angles are concerned, it can be seen from the left side of Figure 7, that the inner air pressure graphs follow a similar pattern, regardless of the wave heading angle. Nevertheless, it should be mentioned that the wave numbers in which oscillations in the air pressure occur, are shifted to higher values as the wave heading angle increases. Concerning the efficiency of the array at several distances from the breakwater, it can be seen (right side of Figure 7) that the examined distances between the devices and the vertical wall cause the array's absorbed power to increase at some $k\alpha$ values and to decrease at another range of wave number compared to the efficiency of five OWCs in isolation condition. This is due to the reflected waves from the wall, which cause a dominant oscillating behavior on the array's absorbed power values. Moreover, as the distance of the OWC from the vertical wall increases, the earlier the oscillatory behavior of the wave absorbed power occurs. As far as the incident wave angles are concerned, it can be obtained that the wave numbers in which oscillations in the power efficiency occur are shifted to higher values as β increases. Finally, it can concluded that the efficiency results for the close to wall distances (i.e., $L_w = 3\alpha, 6\alpha$) follow a more steady pattern, at every examined wave number, compared to the results of the large-distance cases (i.e., $L_w = 9\alpha, 12\alpha$), of which they attain a large oscillatory behavior.

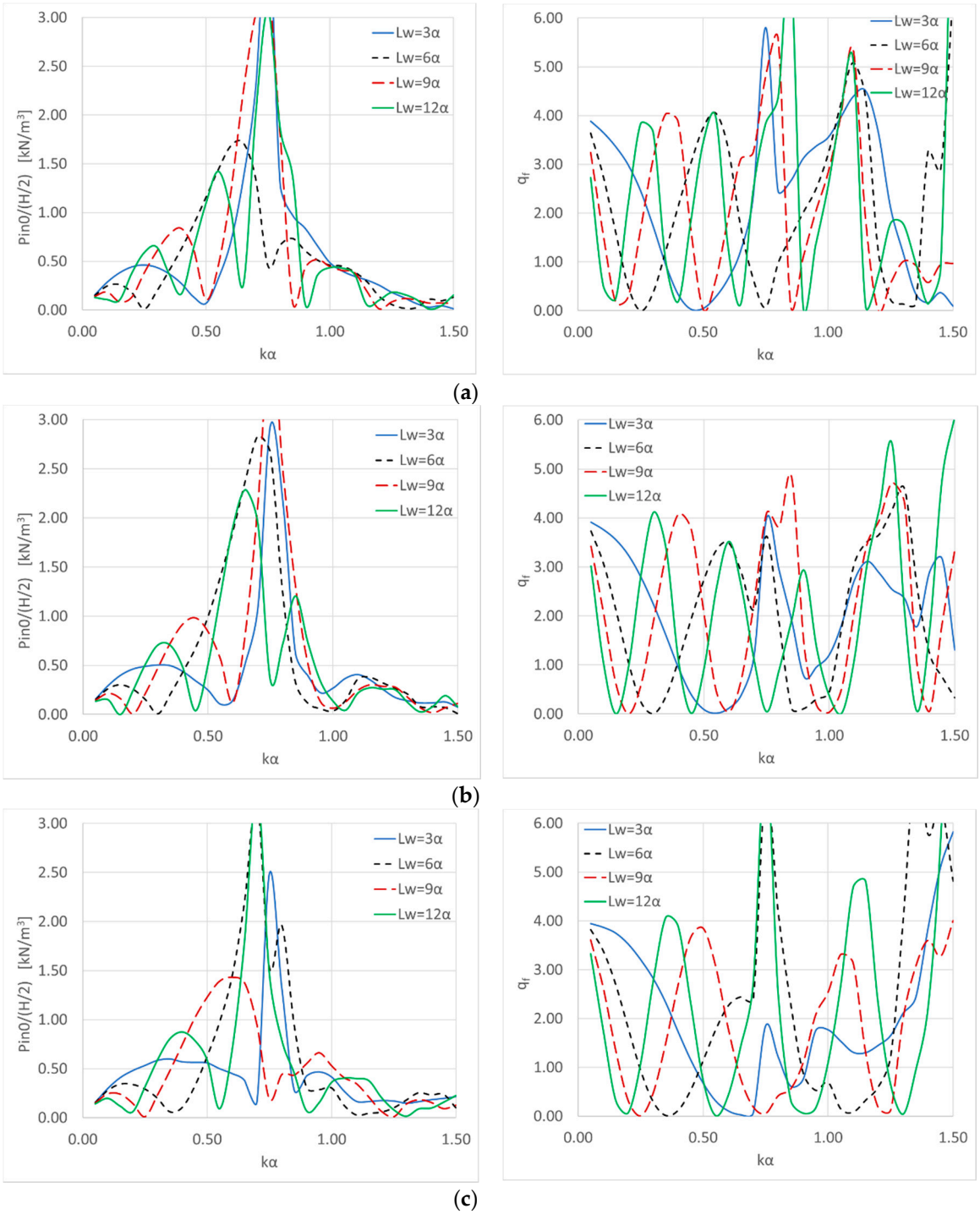

Figure 7. Air pressure inside the 1st OWC (left column figures) and array's q_f factor (right column figures) versus kα for various examined distances between the array and the breakwater and wave heading angles: (**a**) β = 0; (**b**) β = π/6; (**c**) β = π/4.

4.4. Effect of the OWCs' Draught

Next, the effect of the OWCs' draught on their wave power efficiency is examined. Here, also, a parallel arrangement of an array of five similar OWCs in front of a breakwater is considered (see Configuration 5 in Figure 3a). The characteristics of the examined OWCs are presented in Section 4.1, whereas $L_w = 3\alpha$. The examined OWCs' draughts equal to $h_c = 6.14\alpha$, 5.64α, 5.14α, 4.64α, and the wave heading angles to β = 0, π/6, π/4.

Due to the variation of the converter's draught, and consequently to its pumping resonance wave frequency value the air turbine characteristics for the OWC devices equal to: Λ = 10.6; 9.04; 10.47; 18.49 [m^5/(kN.s)] for each examined draught h_c = 6.14α, 5.64α, 5.14α, 4.64α, respectively, for α = 1 m.

Figure 8 depicts the inner air pressure head of the 1st OWC device (left column) and the array's total absorbed power (as presented in Equation (12)), i.e., $P(\omega)/(H/2)^2$, (right column) for various examined OWC draughts and wave heading angles. From the depicted results, it can be seen that the draught of the OWCs affects the inner air pressure head as well as the array's efficiency. Specifically, as the draught of the converter increases, the pumping resonance wave frequency is shifted at lower values, thus the corresponding wave numbers in which the inner air pressure values resonance are transferred to lower values too. Furthermore, it can be noted that as the draught of the OWC increases, the air pressure head inside the 1st OWC decreases. As far as the examined wave heading angles is concerned, it is depicted that β has a minor effect on the inner air pressure head for kα < 0.5. On the other hand, for kα > 0.5, the inner air pressure head inside the 1st OWC decreases as the wave heading angle increases.

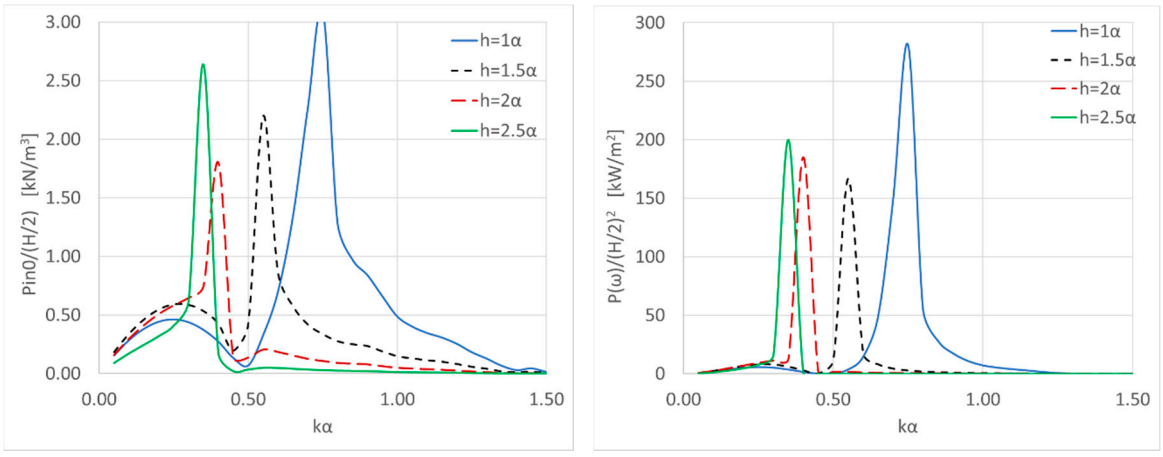

(**a**)

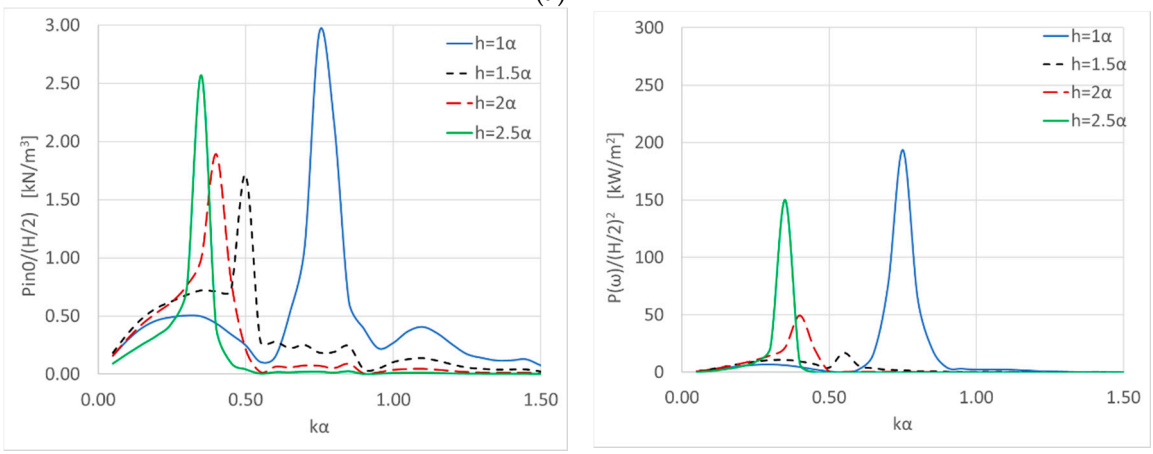

(**b**)

Figure 8. *Cont.*

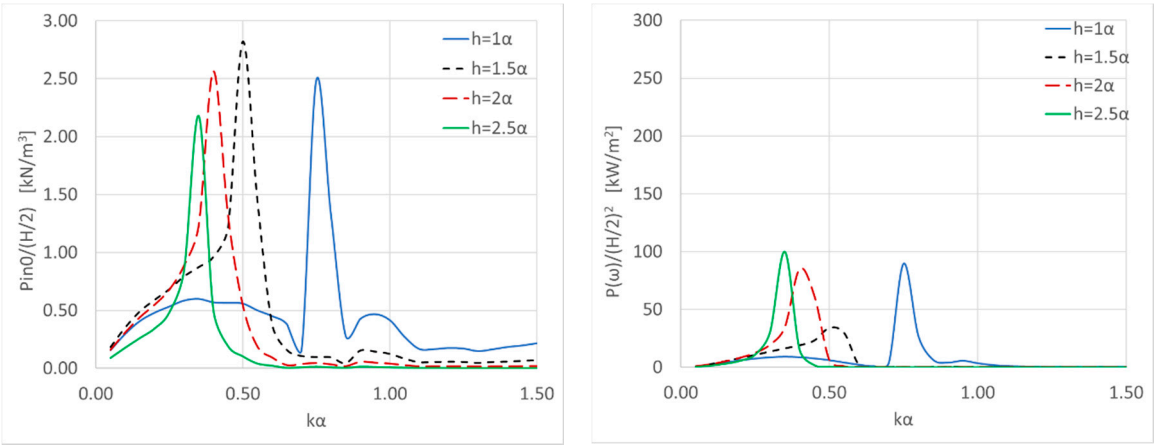

(**c**)

Figure 8. Air pressure inside the 1st OWC (left column figures) and array's absorbed power P(ω) (right column figures) versus kα for various examined OWC draughts and wave heading angles: (**a**) β = 0; (**b**) β = π/6; (**c**) β = π/4.

Concerning the absorbed wave power, it can be seen from the results that the wave numbers in which the absorbed power maximizes (sharp peaks) are not remained constant regardless of the floater's draught, since the wave frequencies at pumping resonance are shifted to lower values. Furthermore, it is noted that the increase of the OWCs' draught has a destructive effect on the array's efficiency as it results in a significant decrease of $P(\omega)$. Concluding, it can be obtained that the increase of the OWCs' draught does not increase the array's efficiency. Contrary, as the draught decreases, the array's absorbed power increases at various wave numbers.

4.5. Effect of the Distance between the OWCs

This subsection examines the effect of the distance between the devices on their wave power efficiency. Here, a parallel arrangement of an array of five similar OWCs in front of a breakwater is considered (see Configuration 5 in Figure 3a). The characteristics of the examined OWCs are presented in Section 4.1. Additionally, the distance between the center of the closest to the wall converter and the breakwater equals to $L_w = 3\alpha$, whereas the distance between the bottom of the external torus and the seabed equals to $h_c = 6.14\alpha$. The air turbine coefficient inside the OWCs equals to 10.60 [m^5/(kN.s)]. Several distances between the converters of the array are examined, i.e., $L_b = 4\alpha$; 8α; 16α; 32α.

Figure 9 depicts the modulus of the air pressure head inside the 1st OWC of the array, as well as the q_f factor for each of the examined distance cases for zero wave heading angle. It can be seen that the inner air pressure of the 1st device seems not to be affected by the distance between the OWCs since similar results are depicted for each examined distance. Furthermore, the presented results follow the same variation pattern regardless the distance between the OWCs in most of the examined wave numbers. It should be noted that the values of the air pressure inside the 1st OWC for the $L_b = 32\alpha$ case are similar to the corresponding values of an isolated OWC in front of a breakwater (see Figure 4a). On the other hand, it can be seen that the q_f factor is significantly affected by the distance between the devices, especially at higher wave frequencies, in which the q_f values appear as an oscillatory behavior (i.e., $k\alpha > 0.7$). This behavior becomes more pronounced as the distance between the adjacent OWCs increases. Contrary, for $k\alpha < 0.7$, the efficiency of the array seems not to be affected by the distance between the devices.

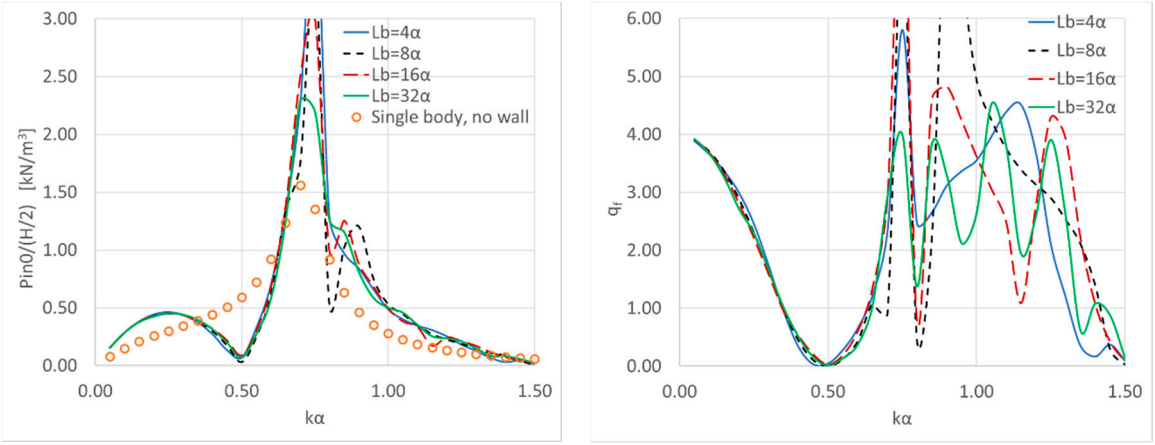

Figure 9. Air pressure inside the 1st OWC (left column figure) and array's q_f factor (right column figure) versus kα for various examined distances between the bodies. Here, β = 0.

5. Conclusions

In this study, the efficiency of an OWC array placed in front of a bottom-mounted, surface piercing, fully reflecting, vertical breakwater is investigated in the frequency domain. The examined OWC-array consists of identical OWC devices containing an exterior partially immersed toroidal body supplemented by a coaxial interior, bottom mounted, free-surface piercing cylinder. In the annulus between the internal cylinder and the external torus, a finite volume air chamber is formed in which the oscillating air pressure is developed. A theoretical formulation based on the image method has been applied to simulate the effect of the vertical wall on the array's power absorption, whereas the wave interaction phenomena between the vertical wall and the converters have been taken into account using the multiple scattering approach.

Three different types of array configurations in front of the vertical wall have been studied, namely a parallel, a perpendicular, and a rectangular arrangement. Furthermore, five types of OWC's arrays configurations have been also examined (i.e., arrays consisting of 1, 2, ..., 5 bodies) for various cases of distances between the devices and the breakwater, wave heading angles, devices' draughts, and distances between adjacent devices. Based on the theoretical computations shown and discussed in the dedicated sections, the main findings of the present research contribution concern the significant effect of the breakwater on the array's efficiency, which is amplified compared to the performance of isolated OWCs (without the presence of the vertical walls). The power performance amplification is strongly affected by the array's orientation to the breakwater; the number of the bodies that consist the array; the wave heading angle; the devices' distance from the breakwater and the devices' draught. Therefore, it can be derived that the installation of an OWC array in front of a vertical breakwater can be an effective way to improve its power absorption efficiency.

However, the infinite wall assumption realized theoretically by the image method should be further examined concerning probable limitations attained at specific wave frequencies. Following the remarks from [55] concerning an array of cylindrical bodies in front of a vertical breakwater, discrepancies between the results of a finite- and an infinite-length breakwater occur. These discrepancies are more pronounced at wave numbers tending to zero, whereas at higher wave numbers, the results from both methods convergence.

The present research will be continued further by determining in the effect of a V-shaped breakwater of a random angle on the power efficiency of an array of OWCs and comparing it with the results of the present study.

Funding: This research received no external funding.

Conflicts of Interest: The authors declare no conflict of interest.

Nomenclature

N	Number of OWC devices
h	Water depth
α	OWC outer radius
b	OWC inner radius
h_c	Distance between the bottom of the external torus and the seabed
c	Radius of the internal cylindrical body
L_w	Distance between the closest to the wall OWC and the vertical wall
L_b	Distance between adjacent OWCs
β	Wave heading angle
ω	Wave frequency
H	Wave height
λ	Wave length
r_k, θ_k, z_k	Local co-ordinate system of the k OWC
Φ	Time harmonic complex velocity potential
φ_0	Velocity potential of the undisturbed incident harmonic wave
φ_s^q	Scattered velocity potential of the q OWC
φ_D^q	Diffraction velocity potential of the q OWC
φ_P^{qp}	Radiation velocity potential resulting from the inner air pressure in p OWC
p_{in0}^p	Amplitude of the oscillating pressure head in the chamber of the p OWC
g	Gravitational acceleration
ρ	Water density
n^q	Unit normal vector
$\delta_{q,p}$	Kronecker's symbol
S_0^q	Mean wetted surface of the q OWC
I	The infinite ring element around the q OWC
II	The ring element below the q OWC
III	The ring element inside the chamber of the q OWC
$Q(t)$	Time dependent air volume flow
u_z	Vertical velocity of the water surface in the OWC
S_i	Cross-sectional area of the inner water surface inside the OWC
q_D^q	Diffraction volume flow of the q OWC
q_p^{qp}	Pressure-dependent volume flow of the q OWC
g_p^{qp}	Radiation conductance of the q OWC
f_p^{qp}	Radiation susceptance of the q OWC
Λ	Complex pneumatic admittance (air turbine coefficient)
Λ_{opt}	Air turbine coefficient optimum value
$P(\omega)$	Absorbed wave power by each OWC of the array
q_f	q-factor term

Appendix A

Starting with the method of separation of variables for the Laplace equation, the velocity potential in each fluid domain, i.e., *I*, *II*, *III* around the q OWC device when it is considered alone in the wave field can be expressed as:

$$\varphi_D^q = -i\omega\frac{H}{2}\sum_{m=-\infty}^{\infty} i^m \Psi_{D,m}^{k,q}\left(r_q, z_q\right)e^{im\theta_q},\ k = I, II, III, \tag{A1}$$

$$\varphi_P^{qp} = \frac{1}{i\omega\rho}\sum_{m=-\infty}^{\infty} \Psi_{P,m}^{k,qp}\left(r_q, z_q\right)e^{im\theta_q},\ k = I, II, III \tag{A2}$$

The expressions of the $\Psi^{q}_{D,m}$, $\Psi^{qp}_{P,m}$ functions in each fluid domain are presented herein, i.e.,: Infinite fluid domain I, ($r_q \geq a,\ 0 \leq z \leq h$):

$$\frac{1}{\delta_j}\Psi^{I,q}_{j,m}\left(r_q, z_q\right) = g^{I,q}_{j,m}\left(r_q, z_q\right) + \sum_{n=0}^{\infty} F^{I,q}_{j,mn}\frac{K_m\left(a_n r_q\right)}{K_m(a_n a)}Z_n(z),\ j = D, P \tag{A3}$$

Here:

$$g^{I,q}_{D,m}\left(r_q, z_q\right) = \left[J_m\left(kr_q\right) - \frac{J_m(ka)}{H_m(ka)}H_m\left(kr_q\right)\right]\frac{Z_0(z)}{d\dot{Z}_0(h)};\ \text{and}\ g^{I,q}_{P,m}\left(r_q, z_q\right) = 0 \tag{A4}$$

In Equations (A3) and (A4), H_m and K_m are the m-th order Hankel function of the first kind and the modified Bessel function of the second type, respectively, while J_m is the m-th order Bessel function of first kind. Additionally, $\delta_D = d;\ \delta_P = 1$. The term $Z_n(z)$ denotes orthonormal function in $[0, h]$ defined as follows:

$$Z_n(z) = \begin{cases} \left[\frac{1}{2}\left[1 + \frac{\sinh(2kh)}{2kh}\right]\right]^{-\frac{1}{2}}\cosh(kz),\ n = 0 \\ \left[\frac{1}{2}\left[1 + \frac{\sin(2a_n h)}{2a_n h}\right]\right]^{-\frac{1}{2}}\cos(a_n z),\ n \geq 1 \end{cases} \tag{A5}$$

Here, the term a_n denotes the positive real roots of the transcendental equation:

$$\frac{\omega^2}{g} + a_n \tan(a_n h) = 0$$

Lower fluid domain II, ($b \leq r_q \leq a; 0 \leq z \leq h_c$):

$$\frac{1}{\delta_j}\Psi^{II,q}_{j,m}\left(r_q, z_q\right) = \sum_{n=0}^{\infty}\varepsilon_n\left(R^{II,q}_{mn}F^{II,q}_{j,mn} + R^{*II,q}_{mn}F^{*II,q}_{j,mn}\right)\cos\left(\frac{n\pi z}{h_c}\right),\ j = D, P \tag{A6}$$

In Equation (A6), $\varepsilon_0 = 1;\ \varepsilon_n = 2,\ n \geq 1$; while:

$$\begin{gathered} R^{II,q}_{mn} = \frac{K_m\left(\frac{n\pi b}{h_c}\right)I_m\left(\frac{n\pi r_q}{h_c}\right) - I_m\left(\frac{n\pi b}{h_c}\right)K_m\left(\frac{n\pi r_q}{h_c}\right)}{K_m\left(\frac{n\pi b}{h_c}\right)I_m\left(\frac{n\pi a}{h_c}\right) - I_m\left(\frac{n\pi b}{h_c}\right)K_m\left(\frac{n\pi a}{h_c}\right)},\ m, n \neq 0 \\ R^{*II,q}_{mn} = \frac{I_m\left(\frac{n\pi a}{h_c}\right)K_m\left(\frac{n\pi r_q}{h_c}\right) - K_m\left(\frac{n\pi a}{h_c}\right)I_m\left(\frac{n\pi r_q}{h_c}\right)}{K_m\left(\frac{n\pi b}{h_c}\right)I_m\left(\frac{n\pi a}{h_c}\right) - I_m\left(\frac{n\pi b}{h_c}\right)K_m\left(\frac{n\pi a}{h_c}\right)},\ m, n \neq 0 \\ R^{II,q}_{m0} = \frac{\left(\frac{r_q}{b}\right)^m - \left(\frac{b}{r_q}\right)^m}{\left(\frac{a}{b}\right)^m - \left(\frac{b}{a}\right)^m},\ m \neq 0,\ n = 0;\ R^{II,q}_{m0} = \frac{\ln\left(\frac{r_q}{b}\right)}{\ln\left(\frac{a}{b}\right)},\ m = n = 0 \\ R^{*II,q}_{m0} = \frac{\left(\frac{a}{r_q}\right)^m - \left(\frac{r_q}{a}\right)^m}{\left(\frac{a}{b}\right)^m - \left(\frac{b}{a}\right)^m},\ m \neq 0,\ n = 0;\ R^{*II,q}_{m0} = \frac{\ln\left(\frac{a}{r_q}\right)}{\ln\left(\frac{a}{b}\right)},\ m = n = 0 \end{gathered} \tag{A7}$$

In Equation (A7), I_m is the m-th order modified Bessel function of first kind.
Inner fluid domain III, ($c \leq r_q \leq a; 0 \leq z \leq h$):

$$\frac{1}{\delta_j}\Psi^{III,q}_{j,m}\left(r_q, z_q\right) = g^{III,q}_{j,m}\left(r_q, z_q\right) + \sum_{i=0}^{\infty}\left(R^{III,q}_{mi}F^{III,q}_{j,mi} + R^{*III,q}_{mi}F^{*III,q}_{j,mi}\right)Z_i(z),\ j = D, P \tag{A8}$$

In Equation (A8), $g^{III,q}_{D,m}\left(r_q, z_q\right) = 0;\ g^{III,q}_{P,m}\left(r_q, z_q\right) = 1$ and:

$$\begin{gathered} R^{III,q}_{mi} = \frac{K_m(a_i c)I_m\left(a_i r_q\right) - I_m(a_i c)K_m\left(a_i r_q\right)}{K_m(a_i c)I_m(a_i b) - I_m(a_i c)K_m(a_i b)},\ R^{III,q}_{mi}(b) = 1,\ R^{III,q}_{mi}(c) = 0,\ m, i \neq 0 \\ R^{*III,q}_{mn} = \frac{I_m(a_i b)I_m\left(a_i r_q\right) - I_m(a_i b)K_m\left(a_i r_q\right)}{K_m(a_i c)I_m(a_i b) - I_m(a_i c)K_m(a_i b)},\ R^{*III,q}_{mi}(b) = 0,\ R^{*III,q}_{mi}(c) = 1,\ m, i \neq 0 \end{gathered} \tag{A9}$$

The terms $F^{I,q}_{j,mn}, F^{II,q}_{j,mn}, F^{*II,q}_{j,mn}, F^{III,q}_{j,mi}, F^{*III,q}_{j,mi}$ in Equations (A3), (A6) and (A8) are Fourier series coefficients.

References

1. Biesheuvel, A.C. Effectiveness of Floating Breakwaters. Master's Thesis, Delft University of Technology, Delft, The Netherlands, 2013.
2. Haggi, A. Report on underwater excavation at the Phoenician Harbour, Atlit, Israel. *Int. J. Naut. Archaeol.* **2010**, *39*, 278–285. [CrossRef]
3. Sadeghi, K.; Abdeh, A.; Al-Dubai, S. An Overview of Construction and Installation of Vertical Breakwaters. *Int. J. Innov. Technol. Explor. Eng.* **2017**, *7*, 1–5.
4. Van der Meer, J.W. Conceptual design of rubble mound breakwaters. *Adv. Coast. Ocean Eng.* **1995**, *1*, 221–315.
5. Goda, Y. *Random Seas and Design of Maritime Structures*, 2nd ed.; World Scientific Publishing: Singapore, 2000.
6. Burcharth, H.F.; Lykke-Andersen, T. Overtopping of rubble mound breakwaters with front reservoir. In Proceedings of the 30th International Conference of Coastal Engineering, San Diego, CA, USA, 3–8 September 2006; pp. 4605–4615.
7. USACE. *Coastal Engineering Manual*; USACE: Washington, DC, USA, 2002.
8. Vicinanza, D.; Lauro, E.D.; Contestabile, P.; Gisonni, C.; Lara, J.L.; Losada, I.J. Review of Innovative Harbor Breakwaters for Wave-Energy Conversion. *J. Waterw. Port Coast. Ocean Eng.* **2019**, *145*, 03119001. [CrossRef]
9. Contestabile, P.; Crispino, G.; Russo, S.; Gisonni, C.; Cascetta, F.; Vicinanza, D. Crown wall modifications as response to wave overtopping under a future sea level scenario: An experimental parametric study for an innovative composite seawall. *Appl. Sci.* **2020**, *10*, 2227. [CrossRef]
10. Lee, B.W.; Park, W.-S. Evaluation of the Hydraulic Performance of a Rear-Parapet Vertical Breakwater under Regular Waves through Hydraulic Experiments. *Water* **2020**, *12*, 2428. [CrossRef]
11. Park, W.S.; Seo, J.; Won, D.; Lee, B.W. Stability assessment formulas for an interlocking caisson breakwater under oblique wave conditions. *J. Coast. Res.* **2018**, *85*, 1236–1240. [CrossRef]
12. Hu, P. Dynamic responses analysis of permeable breakwater subjected to random waves. *Adv. Mater. Res.* **2015**, *1061–1062*, 809–812.
13. Elkotby, M.; Rageh, O.; Sarhan, T.; Ezzeldin, M. Wave transformation behind permeable breakwater. *Int. J. Sci. Eng. Res.* **2019**, *10*. [CrossRef]
14. Yoo, J.; Kim, S.-Y.; Kim, J.-M.; Cho, Y.-S. Experimental Investigation of the Hydraulic Performance of Caisson-Pile Breakwaters. *J. Coast. Res.* **2010**, *263*, 444–450. [CrossRef]
15. Pourteimouri, P.; Hejazi, K. Development of An Integrated Numerical Model for Simulating Wave Interaction with Permeable Submerged Breakwaters Using Extended Navier–Stokes Equations. *J. Mar. Sci. Eng.* **2020**, *8*, 87. [CrossRef]
16. Mellink, B. Numerical and Experimental Research of Wave Interaction with a Porous Breakwater. Master's Thesis, TU Delft, Delft, The Netherlands, 2012.
17. Kralli, V.E.; Theodossiou, N.; Karambas, T. Optimal Design of Overtopping Breakwater for Energy Conversion (OBREC) Systems Using the Harmony Search Algorithm. *Front. Energy Res.* **2019**, *7*. [CrossRef]
18. Contestabile, P.; Ferrante, V.; Di Lauro, E.; Vicinanza, D. Prototype overtopping breakwater for wave energy conversion at port of Naples. In Proceedings of the 26th International Ocean and Polar Engineering Conference (ISOPE 2016), Rhodes, Greece, 26 June–2 July 2016; pp. 616–621.
19. Gravas, A.; Savvidis, Y.; Koutitas, C. Modelling study of wave energy harnessing port structures. *Fresenius Environ. Bull.* **2012**, *21*, 3069–3076.
20. Vicinanza, D.; Margeritini, L.; Kofoed, J.P.; Buccino, M. The SSG wave energy converter: Performance, status and recent developments. *Energies* **2012**, *5*, 193–226. [CrossRef]
21. Cabral, T.; Clemente, D.; Rosa-Santos, P.; Taveira-Pinto, F.; Morais, T.; Belga, F.; Cestaro, H. Performance Assessment of a Hybrid Wave Energy Converter Integrated into a Harbor Breakwater. *Energies* **2020**, *13*, 236. [CrossRef]
22. Sarkar, D.; Renzi, E.; Dias, F. Effect of a straight coast on the hydrodynamics and performance of the Oscillating Wave Surge Converter. *Ocean Eng.* **2015**, *105*, 25–32. [CrossRef]
23. Michele, S.; Sammarco, P.; Errico, M. The optimal design of a flap gate array in front of a straight vertical wall: Resonance of the natural modes and enhancement of the existing torque. *Ocean Eng.* **2016**, *118*, 152–164. [CrossRef]
24. Cascajo, R.; Garcia, E.; Quiles, E.; Correcher, A.; Morant, F. Integration of marine wave energy converters into seaports: A case study in port of Valencia. *Energies* **2019**, *12*, 787. [CrossRef]

25. Konispoliatis, D.N.; Mavrakos, S.A.; Katsaounis, G.M. Theoretical evaluation of the hydrodynamic characteristics of arrays of vertical axisymmetric floater of arbitrary shape in front of a vertical breakwater. *J. Mar. Sci. Eng. Res.* **2020**, *8*, 62. [CrossRef]
26. Konispoliatis, D.N.; Mavrakos, S.A. Wave power absorption by arrays of wave energy converters in front of a vertical breakwater: A theoretical study. *Energies* **2020**, *13*, 1985. [CrossRef]
27. Martins-rivas, H.; Mei, C.C. Wave power extraction from an oscillating water column at the tip of a breakwater. *J. Fluid Mech.* **2009**, *626*, 395–414. [CrossRef]
28. Martins-rivas, H.; Mei, C.C. Wave power extraction from an oscillating water column along a straight coast. *Ocean Eng.* **2009**, *36*, 426–433. [CrossRef]
29. Zheng, S.; Zhang, Y.; Inglesias, G. Coast/breakwater-integrated OWC: A theoretical model. *Mar. Struct.* **2019**, *66*, 121–135. [CrossRef]
30. Viviano, A.; Naty, S.; Foti, E.; Bruce, T.; Allsop, W.; Vicinanza, D. Large-scale experiments on the behavior of a generalized oscillating water column under random waves. *Renew. Energy* **2016**, *99*, 875–887. [CrossRef]
31. Howe, D.; Nader, J.R. OWC WEC integrated within a breakwater versus isolated: Experimental and numerical theoretical study. *Int. J. Mar. Energy* **2017**, *20*, 165–182. [CrossRef]
32. Naty, S.; Viviano, A.; Foti, E. Wave energy exploitation system integrated in the coastal structure of a Mediterranean port. *Sustainability* **2016**, *8*, 1342. [CrossRef]
33. Naty, S.; Viviano, A.; Foti, E. Feaseability study of a wec integrated in the port of giardini naxos, Italy. In Proceedings of the 35th Conference on Coastal Engineering, Antalya, Turkey, 17–20 November 2016.
34. Zheng, S.; Antonini, A.; Zhang, Y.; Greaves, D.; Miles, J.; Iglesias, G. Wave power extraction from multiple oscillating water columns along a straight coast. *J. Fluid Mech.* **2019**, *878*, 445–480. [CrossRef]
35. Park, S.; Kim, K.H.; Nam, B.W.; Kim, J.S.; Hong, K. A Study on Effects of Breakwater on Performance of OWC. In Proceedings of the 13th International Society of Offshore and Polar Engineers Symposium, (ISOPE), Jeju, Korea, 14–17 October 2018.
36. Tsai, C.P.; Ko, C.H.; Chen, Y.C. Investigation on Performance of a Modified Breakwater-Integrated OWC Wave Energy Converter. *Sustainability* **2018**, *10*, 643. [CrossRef]
37. Konispoliatis, D.; Mavrakos, S. Theoretical performance investigation of a vertical cylindrical oscillating water column device in front of a vertical breakwater. *J. Ocean Eng. Mar. Energy* **2019**. [CrossRef]
38. Konispoliatis, D.; Mavrakos, S.A.; Soukissian, T.H. Array of oscillating water column devices in front of a vertical breakwater in the Mediterranean Sea. In Proceedings of the 12th International Conference on Deregulated Electricity Market Issues in Southern Eastern Europe (DEMSEE 2019), Herakleion, Greece, 19–20 September 2019.
39. Zhou, Y.; Zhang, C.; Ning, D. Hydrodynamic Investigation of a Concentric Cylindrical OWC Wave Energy Converter. *Energies* **2018**, *11*, 985. [CrossRef]
40. Michele, S.; Renzi, E.; Perez-Collazo, C.; Greaves, D.; Iglesias, G. Power extraction in regular and random waves from an OWC in hybrid wind-wave energy systems. *Ocean Eng.* **2019**, *191*, 106519. [CrossRef]
41. Perez-Collazo, C.; Greaves, D.; Iglesias, G. A Novel Hybrid Wind-Wave Energy Converter for Jacket-Frame Substructures. *Energies* **2018**, *11*, 637. [CrossRef]
42. Qiao, D.; Feng, C.; Ning, D.; Wang, C.; Liang, H.; Li, B. Dynamic response analysis of Jacket platform integrated with oscillating water column device. *Front. Energy Res.* **2020**. [CrossRef]
43. Falnes, J.; McIver, P. Surface wave interactions with systems of oscillating bodies and pressure distributions. *Appl. Ocean Res.* **1985**, *7*, 225–234. [CrossRef]
44. Yeung, R.W.; Sphaier, S.H. Wave-interference effects on a truncated cylinder in a channel. *J. Eng. Math.* **1989**, *23*, 95–117. [CrossRef]
45. Kokkinowrachos, K.; Mavrakos, S.A.; Asorakos, S. Behaviour of vertical bodies of revolution in waves. *Ocean Eng.* **1986**, *13*, 505–538. [CrossRef]
46. Konispoliatis, D.; Mavrakos, S. Hydrodynamic analysis of an array of interacting free-floating oscillating water column (OWC's) devices. *Ocean Eng.* **2016**, *111*, 179–197. [CrossRef]
47. Evans, D.V. Wave-power absorption by systems of oscillating surface pressure distributions. *J. Fluid Mech.* **1982**, *114*, 481–499. [CrossRef]
48. Sarmento, A.J.N.A.; Falcao, A.F.O. Wave generation by an oscillating surface-pressure and its application in wave-energy extraction. *J. Fluid Mech.* **1985**, *150*, 467–485. [CrossRef]

49. Evans, D.V.; Porter, R. Efficient calculation of hydrodynamic properties of O.W.C type devices. In Proceedings of the 15th Offshore Mechanics and Arctic Engineering (OMAE 1996), Florence, Italy, 16–20 June 1996; Part B. pp. 123–132.
50. Mavrakos, S.A.; McIver, P. Comparison of methods for computing hydrodynamic characteristics of arrays of wave power devices. *Appl. Ocean Res.* **1997**, *19*, 283–291. [CrossRef]
51. Falnes, J. *Ocean Waves and Oscillating Systems: Linear Interactions Including Wave-Energy Extraction*; Cambridge University Press: Cambridge, UK, 2002.
52. Mavrakos, S.A. *User's Manual for the Software HAMVAB*; School of Naval Architecture and Marine Engineering, Laboratory for Floating Structures and Mooring Systems: Athens, Greece, 1995.
53. Faltinsen, O.M. *Sea Loads on Ships and Offshore Structures*; Cambridge University Press: Cambridge, UK, 1990.
54. Silverman, S.; Abramson, H.N. *Lateral Sloshing in Moving Containers. The Dynamic Behavior of Liquids in Moving Containers*; Abramson, N.H., Ed.; NASA SP-106; NASA: Washington, DC, USA, 1966; p. 13. 467p.
55. Loukogeorgaki, E.; Chatjigeorgiou, I.K. Hydrodynamic Performance of an Array of Wave Energy Converters in Front of a Vertical Wall. In Proceedings of the 13th European Wave and Tidal Energy Conference (EWTEC 2019), Napoli, Italy, 1–6 September 2019; p. 1464.